NANO LETTERS

Letter

pubs.acs.org/NanoLett

Crossover from 3D to 2D Quantum Transport in Bi_2Se_3/In_2Se_3 Superlattices

Yanfei Zhao,[†,‡,¶] Haiwen Liu,[†,‡,¶] Xin Guo,[§] Ying Jiang,[∥] Yi Sun,[†,‡] Huichao Wang,[†,‡] Yong Wang,[∥] Han-Dong Li,[⊥] Mao-Hai Xie,*[,§] Xin-Cheng Xie,*[,†,‡] and Jian Wang*[,†,‡]

[†]International Center for Quantum Materials, School of Physics, Peking University, Beijing 100871, People's Republic of China

[‡]Collaborative Innovation Center of Quantum Matter, Beijing 100871, People's Republic of China

[§]Physics Department, The University of Hong Kong, Hong Kong, People's Republic of China

[∥]Center of Electron Microscopy, State Key Laboratory of Silicon Materials, Department of Materials Science and Engineering, Zhejiang University, Hangzhou 310027, People's Republic of China

[⊥]State Key Laboratory of Electronic Thin Films and Integrated Devices, University of Electronic Science and Technology of China, Chengdu 610054, People's Republic of China

Supporting Information

ABSTRACT: The topological insulator/normal insulator (TI/NI) superlattices (SLs) with multiple Dirac channels are predicted to offer great opportunity to design novel materials and investigate new quantum phenomena. Here, we report first transport studies on the SLs composed of TI Bi_2Se_3 layers sandwiched by NI In_2Se_3 layers artificially grown by molecular beam epitaxy (MBE). The transport properties of two kinds of SL samples show convincing evidence that the transport dimensionality changes from three-dimensional (3D) to two-dimensional (2D) when decreasing the thickness of building block Bi_2Se_3 layers, corresponding to the crossover from coherent TI transport to separated TI channels. Our findings provide the possibility to realizing "3D surface states" in TI/NI SLs.

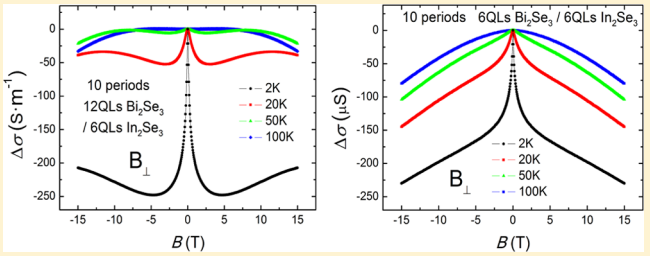

KEYWORDS: *topological insulators, superlattices, transport dimensionality, weak-localization, weak-antilocalization*

The discovery of topological insulators (TIs) has gained wide interest owing to its topologically nontrivial property.[1−3] The extraordinary property of the 2D topological surface states of TIs is exemplified by the absence of backscattering by nonmagnetic impurities and weak antilocalization (WAL) of the Dirac Fermions.[4−14] Remarkably, recent theoretical studies have demonstrated that such topological protected surface states are the 2D version of Weyl electron. As for 3D, Weyl semimetal possessing "3D surface states" can be achieved in superlattices (SLs) where TIs are interlaced with normal insulators (NIs).[15−17]

Semiconductor SL engineering is a common strategy to modulate the quantum states by controlling various parameters such as altering the stacking sequence of layers or the thickness of stacking layers.[18,19] The expectation is that SLs composed of known TI and NI by tuning the thickness of TI layers can induce different quantum behavior, even leading to the change of topological class. This has been investigated in the natural multilayer systems $(PbSe)_5(Bi_2Se_3)_{3m}$[20] and $(Bi_2)_1(Bi_2Se_3)_1$ by ARPES.[21,22] Due to the limitation of the photoemission technique, thus far, the study of these natural multilayer systems are only focused on the top surface of SLs. The scarcity of transport experiments hinders an in-depth understanding of the physical properties in TI/NI SLs. In addition, compared to the natural multilayer heterostructure, the molecular beam epitaxy (MBE) technique provides an effective route to construct SLs artificially. Either the stacking sequence or the thickness of layers of SL structures can be accurately controlled, which may trigger various quantum phenomena.[23] Therefore, it is highly desirable to demonstrate the transport properties of the artificial TI/NI SLs grown by MBE.

In our study, we investigate the transport property of SL heterostructure consisted of alternating Bi_2Se_3 and In_2Se_3 layers grown on insulating substrates by MBE.[24] Two kinds of SLs are measured. One is 10 periods of 12 quintuple layers (QLs) Bi_2Se_3/6 QLs In_2Se_3 SLs on nonmagnetic Fe-doped semi-insulating InP(111) substrate (resistivity $\rho \geq 10^7\Omega$·cm at room temperature) and the other is 10 periods of 6 QLs Bi_2Se_3/6 QLs In_2Se_3 SLs on undoped, highly resistive Si(111) substrate ($\rho \geq 10^4\Omega$·cm at room temperature). Through theoretical analysis and quantitative fitting of the experimental results, we confirm that SLs with different thickness of TI layers display obviously different quantum behavior. For the 12 QLs Bi_2Se_3/6 QLs In_2Se_3 SLs, the transport behavior can be well explained by

Received: June 13, 2014
Revised: July 28, 2014
Published: August 7, 2014

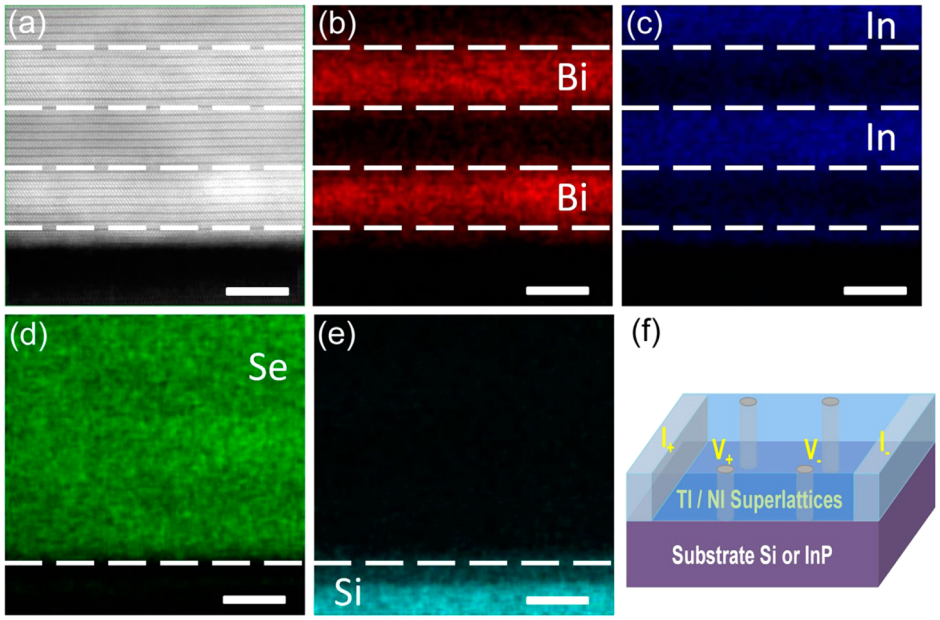

Figure 1. Transmission electron microscopy. (a) High angle annular dark field scanning transmission electron microscopy (HAADF-STEM) image of the $(Bi_2Se_3)_6/(In_2Se_3)_6$ SL structure. (b)−(e) EDX elemental mapping of Bi, In, Se and Si, respectively. The white dashed lines indicate the interface of Bi_2Se_3, In_2Se_3 and the substrate Si. Scale bars represent 7 nm. (f) Schematic structure for the transport measurements in the TI/NI SLs. The thickness is not to scale.

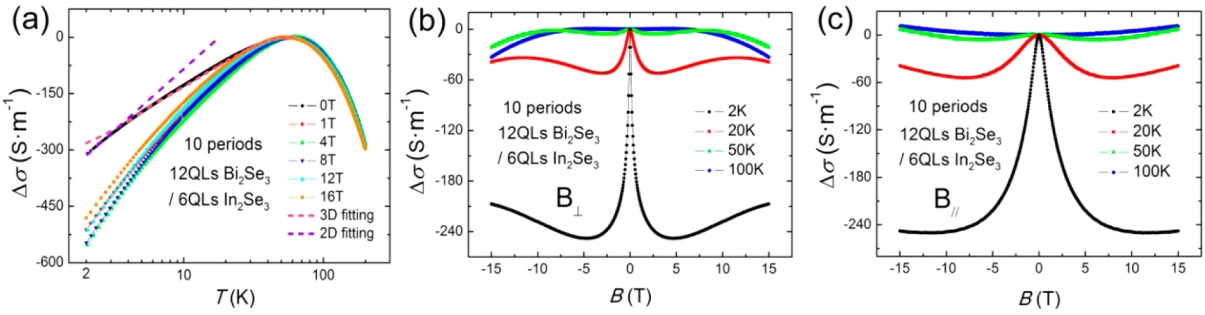

Figure 2. Transport measurements of $(Bi_2Se_3)_{12}/(In_2Se_3)_6$ SLs. (a) Temperature dependence of normalized longitudinal conductivity of $(Bi_2Se_3)_{12}/(In_2Se_3)_6$ SLs at different magnetic fields. The violet dashed line is the 2D theory fitting, whereas the pink one is the 3D theory fitting. (b) Normalized MC vs magnetic field of $(Bi_2Se_3)_{12}/(In_2Se_3)_6$ SLs measured in the perpendicular field at different temperatures. (c) Normalized MC as a function of parallel field at different temperatures.

anisotropic 3D WAL combined with 3D electron−electron interaction (EEI) theory. This feature indicates the TI layers in SLs are coherently coupled and electrons can diffuse to the neighboring planes exhibiting 3D anisotropic behavior. In contrast, for the 6 QLs Bi_2Se_3/6 QLs In_2Se_3 SLs, the transport behavior can be simply explained by 2D WAL model combined with 2D EEI, indicating the electrons are confined in 2D transport channels and the system behaves just like a stack of incoherent 2D metallic planes. Our results clearly demonstrate that tuning the thickness of TI layers may completely influence the transport dimensionality in Bi_2Se_3/In_2Se_3 SLs.

The Bi_2Se_3/In_2Se_3 SL structures are grown on Si(111) and InP(111) substrates in a customized MBE system with the base pressure of 2×10^{-10} Torr, where indium (In), bismuth (Bi), and selenium (Se) fluxes are evaporated from Knudsen cells.[24] The flux ratio between In and Bi is 1:10, and the film growth rate is 3 QLs/min. The deposition temperature is ∼200 °C. In situ reflection high energy electron diffraction (RHEED) is applied to monitor the growing surfaces in real-time to assess the film growth mode, lattice misfit strain, and surface reconstructions. The SL structures are synthesized by repeating 10 times of the layers comprising of m QLs Bi_2Se_3 and n QLs In_2Se_3. In the following, the SLs are expressed as $(Bi_2Se_3)_m/(In_2Se_3)_n$, which means m QLs of Bi_2Se_3 sandwiched by adjacent n QLs of In_2Se_3. We performed the experiments for a fixed n value (n = 6) with m = 12 ($(Bi_2Se_3)_{12}/(In_2Se_3)_6$ SLs) and m = 6 ($(Bi_2Se_3)_6/(In_2Se_3)_6$ SLs).

The SL structures are examined by a FEI TITAN Cs-corrected cross-sectional scanning transmission electron microscopy (STEM) operating at 200 kV. Figure 1a shows a high angle annular dark field scanning transmission electron microscopy (HAADF-STEM) image of the $(Bi_2Se_3)_6/(In_2Se_3)_6$ SL structure. The light layers in the image represent Bi_2Se_3 due to a larger atomic number of Bi (Z = 83),[25] whereas In_2Se_3 layers appear relatively dark because of the smaller atomic number of In (Z = 49). The interfaces between Bi_2Se_3 and In_2Se_3 layers are indicated by white dashed lines shown in Figure 1a. Further, the colored energy dispersive X-ray spectroscopy (EDX) maps collected from the SLs (Bi, In and Se) and substrate Si are illustrated individually in Figure 1b−e,

dx.doi.org/10.1021/nl502220p | Nano Lett. 2014, 14, 5244−5249

which are all in agreement with our sample features, illustrating the high quality of our samples.

As shown in Figure 1f, standard six-terminal Hall-bar geometry is used to measure the SL samples. Two indium current electrodes (I^+ and I^-) are pressed on both ends and across the entire width of the SLs, so that the current can homogeneously go through the SLs in longitudinal direction. The other four indium electrodes were pressed on the SLs as voltage probes (see Methods in Supporting Information). Figure 2a shows the temperature dependence of conductivity $\Delta\sigma(T) = \sigma(T) - \sigma(T_0)$ for $(Bi_2Se_3)_{12}/(In_2Se_3)_6$ sample, where T_0 is a reference temperature at which the conductivity reaches maximum. With decreasing the temperature (T), the conductivity curves at different magnetic fields always exhibit a maximum peak at about 60 K and then show an obvious decrease. This behavior is basically correlated to the WAL effect and EEI.[26] Figure 2b displays the MC $\Delta\sigma(B) = \sigma(B) - \sigma(0)$ of $(Bi_2Se_3)_{12}/(In_2Se_3)_6$ measured at varied temperatures in perpendicular field. At T = 2 K, magneto-conductivity (MC) shows a sharp negative cusp in low field regime and rapidly decreases with increasing field. At around 4.7 T, MC reaches the minimum and then starts to increase at higher field. When increasing T (T = 20, 50, 100 K curves in Figure 2b), the sharp cusp, characteristic of WAL, is eventually suppressed. More interestingly, the crossover field, where the MC switches from negative to positive, becomes smaller at higher T. The overall MC evolution reveals that, the crossover feature remains as T increases, and the low field WAL cusp and high field weak localization (WL) behavior become less pronounced simultaneously.

The MC measured in parallel field (in-plane and always perpendicular to the electric current) shows similar features. The typical temperature evolution of the parallel MC curves of $(Bi_2Se_3)_{12}/(In_2Se_3)_6$ SLs are shown in Figure 2c. At low T, the low field MC shows the negative WAL behavior, while in high field, it tends to exhibit a slightly upturn indicating the tendency toward WL. At higher T, the WAL to WL crossover becomes more pronounced. It is worth noting that at certain fixed temperature, the crossover field in parallel field is larger than that in perpendicular field.

All the transport behaviors shown in Figure 2 cannot be explained by the 2D theory. First, the $\sigma(T)$ at zero field displays the conductivity decrease diverging from the logarithmic T–dependence, which is inconsistent with the 2D theory[26,27] (shown by the violet dashed line in Figure 2a). Second, the amplitude of conductivity decrease with decreasing temperature is larger than that in 2D TI films,[26−28] indicating different transport mechanism. Moreover, contrasting to the typical 2D WAL behavior obtained in various TIs films,[5,8,11] the observed crossover from WAL to WL (Figure 2b and c) is distinctive. In previous experiments, the crossover features have been observed in magnetically doped TI films[29−31] and undoped ultrathin TI thin films (<6 QLs),[32,33] both of which can be explained by 2D theory due to the crossover field is less than 1 T. However, the systems here are nonmagnetic doping SL structures with relatively thick unit films (≥6 QLs) and the crossover field is about 5 T; therefore, these two possibilities, as well as the 2D explanation of conductivity corrections, are ruled out. In short, both temperature dependence conductivity and the crossover behavior of MC in $(Bi_2Se_3)_{12}/(In_2Se_3)_6$ SLs reveal the inapplicability of 2D theory to describe the transport mechanism and imply a different physical origin, which stems from the unique Bi_2Se_3/In_2Se_3 SL structures.

To account for the nonlinear negative conductivity correction $\Delta\sigma(T)$ vs ln T curve at zero field, a 3D WAL model combined with 3D EEI is utilized. The total quantum correction to conductivity can be expressed as[34]

$$\begin{aligned}\Delta\sigma(T) &= \Delta\sigma_{WAL}(T) + \Delta\sigma_{EEI}(T)\\ &= -\frac{\delta e^2}{2\hbar\pi^3 L_0}[(T/T_0)^{p/2} - 1]\\ &\quad + \frac{1.3e^2}{4\hbar\pi^2}\sqrt{\frac{k_B T_0}{2\hbar D_{||}}}\left(\frac{4}{3} - \frac{3}{2}\tilde{F}_\sigma\right)(\sqrt{T/T_0} - 1)\end{aligned} \quad (1)$$

In eq 1, the formula has two competing contributions. The first term$\Delta\sigma_{WAL}(T)$ represents the increase of conductivity by 3D WAL. Here, δ describes the anisotropy factor of the SLs system, L_0 denotes the dephasing length at the maximum conductivity temperature T_0, and $D_{||}$ is the in-plane diffusion constant. The second term $\Delta\sigma_{EEI}(T)$ denotes the suppression of conductivity by EEI. $\tilde{F}_\sigma$ is the screening factor. L_0/δ and $\tilde{F}_\sigma$ are two independent fitting parameters. As shown in Figure 2a by pink dashed line, the fitting yields L_0/δ = 9.5 nm and $\tilde{F}_\sigma$= 0.43. (Fitting details are in Supporting Information) Our experimental data are quantitatively in agreement with the fitting, indicating that the electrons in $(Bi_2Se_3)_{12}/(In_2Se_3)_6$ SLs exhibit the 3D coherent transport between neighboring layers rather than confined in 2D layers.

The influence of the magnetic field orientation on $(Bi_2Se_3)_{12}/(In_2Se_3)_6$ SLs magnetotransport is depicted in Figure 3. The amplitude of $\Delta\sigma(B)$ in the perpendicular field

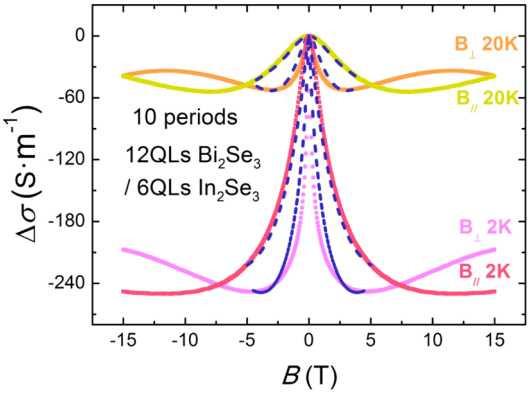

Figure 3. Anisotropic magnetoconductivity of $(Bi_2Se_3)_{12}/(In_2Se_3)_6$ SLs. Conductivity vs magnetic field plot of $(Bi_2Se_3)_{12}/(In_2Se_3)_6$ SLs sample in both perpendicular and parallel field at T = 2 and 20 K. The dark blue dashed curves are the fittings using 3D WAL model combined with 3D EEI by eq 2.

is almost the same with that measured in the parallel field. This is different from the MC behavior measured in 2D TI thin films,[26,27] where $\Delta\sigma(B)$ measured in the parallel field is much smaller than the perpendicular field setup. Moreover, as shown in Figure 3, the broader WAL regime in parallel field, as well as the larger crossover field, suggests the anisotropy behavior in $(Bi_2Se_3)_{12}/(In_2Se_3)_6$ SLs. Besides, the negative conductivity correction (shown in Figure 2a) manifests that EEI also contributes to the MC corrections. On the basis of 3D anisotropic WAL model combined with 3D EEI, the corresponding quantum MC correction reads[34,35]

dx.doi.org/10.1021/nl502220p | Nano Lett. 2014, 14, 5244−5249

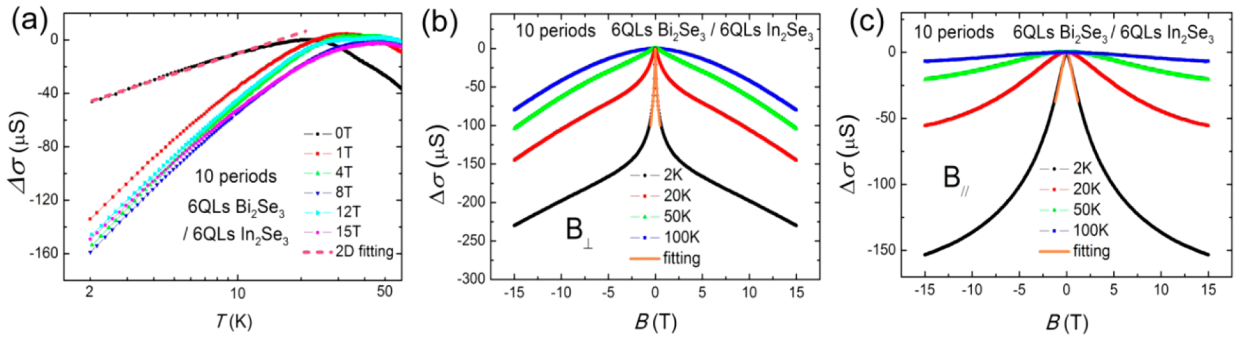

Figure 4. Transport measurements of $(Bi_2Se_3)_6/(In_2Se_3)_6$ SLs. (a) Conductivity vs temperature measured of $(Bi_2Se_3)_6/(In_2Se_3)_6$ SLs at different magnetic fields. The pink dashed line represents the fitting to 2D WAL combined with EEI model. Normalized MC vs magnetic field measured in the perpendicular (b) and parallel field (c) at different temperatures. The orange solid lines show the fitting results with eq 4 and 5

$$\Delta\sigma_i(H) = -\delta\frac{e^2}{2\pi^2\hbar}\sqrt{\frac{eB}{\hbar}}\left[\frac{1}{2}f_3\left(\alpha_i\frac{B}{B_\phi}\right) - \frac{3}{2}f_3\left(\alpha_i\frac{B}{B_\phi + 4/3B_{SO}}\right)\right] - \frac{e^2}{4\pi^2\hbar}\tilde{F}_\sigma\sqrt{\frac{k_BT}{2\hbar D_\parallel}}g_3(h) \quad (2)$$

The first term in eq 2 denotes the WAL-WL corrections and the second term is the EEI correction. The subscript i of σ and α represents ∥ and ⊥, indicating the orientation of the magnetic field (parallel and perpendicular to the plane of film, respectively). In the Kawabata function $f_3(x)$, the prefactors satisfy $\alpha_\parallel = \delta^{-2}$ and $\alpha_\perp = 1$.[35] (More details are in Supporting Information.) $B_\phi = \hbar/4eL_\varphi^2$ and $B_{SO} = \hbar/4eL_{SO}^2$ are two characteristic fields related to the phase coherence length and spin orbit flip length. In the EEI correction part, the function $g_3(h)$ satisfies $g_3(h) = \int_0^\infty d\varepsilon[(\varepsilon + h)^{1/2} + (|\varepsilon - h|)^{1/2} - 2\sqrt{\varepsilon}]d^2(\varepsilon/(e^{\beta\varepsilon} - 1))/d\varepsilon^2$ with $h = \beta g\mu_B B$ and $\beta = (k_BT)^{-1}$. The screening factor $\tilde{F}_\sigma$ is fixed to be 0.43 yielding from the fitting results of eq 1. Thus, δ, L_φ, and L_{SO} are three fitting parameters in eq 2. Commonly, the fitting range for 3D theory is larger than 2D theory.[36,37] Here, the fitting range is about 5 T to −5 T to capture the crossover features. As shown by the dashed lines in Figure 3, the MC behaviors were quantitatively in accordance with the 3D theory over a range of −5 to 5 T in both perpendicular and parallel field. Extracting from eq 2, we obtain the fitting parameters: $\delta = \sqrt{2.2}$, $L_\varphi \approx 204$ nm, and $L_{SO} \approx 21.7$ nm at 2 K and $\delta = \sqrt{2.2}$, $L_\varphi \approx 51.0$ nm, and $L_{SO} \approx 20.6$ nm at 20 K.

In the SLs system with strong spin−orbit coupling (SOC) and EEI, the phase coherence length L_φ, the spin orbit flip length L_{SO} and the magnetic length L_B are three main characteristic lengths, which are dominant parameters for quantum interference properties. Basically, from eq 2, negative MC correction comes from suppressing the spin-singlet Cooperon channel (characterized by L_φ), whereas a positive MC correction is owing to the inhibition of spin-triplet Cooperon channel (mainly characterized by L_{SO}).[34] According to the fitting results, at low T, the system generally has $L_{SO} \ll L_\varphi$. In the low field, $L_B = (\hbar/4eB)^{1/2}$ is much larger than L_φ and L_{SO}, and the spin-singlet Cooperon channel is gradually being suppressed with increasing the magnetic field, thus, the system shows WAL dominate feature. When increasing the magnetic field to $L_{SO} < L_B < L_\varphi$, not only the spin-singlet but also the spin-triplet Cooperon channels began to be suppressed, leading to the competing behavior between WAL and WL. At higher field, L_B is further reduced to $L_B < L_{SO}$, the spin-singlet channel is totally suppressed. The positive MC appears as a WL dominate feature. Overall, with increasing the magnetic field, MC displays the crossover from WAL to WL when $L_B \approx L_{SO}$. However, what is the physical mechanism underlies the crossover behavior? We propose that the possible explanation is the coupled TI layer transport in SL structures. The coherence of the electron is closely linked to the quantum interference behavior. The surface states of TI films hybridize with the bulk quantum well states, diffuse into the neighboring SL layers, and give rise to 3D WAL features at low magnetic field. The hybridization of surface and bulk states results in a finite effective spin−orbital coupling strength, and leads to the 3D WAL to WL crossover at high magnetic field. Thus, the system presents a complicated combination of surface and bulk states with competing behavior between WAL and WL. On the other hand, the magnetic field leads to Zeeman splitting between spin triplet diffusion channels and introduces remarkable MC corrections to the EEI contribution at low temperature.[34] Furthermore, in a 3D SLs system with strong SOC and EEI, the anisotropy of the MC behavior is anticipated due to the anisotropic effective mass of $(Bi_2Se_3)_{12}/(In_2Se_3)_6$ TI SLs. As shown in Figure 3, for a fixed T, the crossover field in the parallel field is about 2.2 times larger than that in the perpendicular field, which is consistent with anisotropic factor $\delta^2 = 2.2$.

Therefore, the anisotropic 3D WAL theory combined with 3D EEI nicely reproduces the transport behaviors of $(Bi_2Se_3)_{12}/(In_2Se_3)_6$ SLs. The layers in $(Bi_2Se_3)_{12}/(In_2Se_3)_6$ SLs are coherently coupled and the electrons may diffuse into the neighboring planes exhibiting 3D anisotropic behavior.

To gain further insights into the unusual transport behavior in SL structures, we reduce the thickness of Bi_2Se_3 layers to six QLs to see whether it will possess different transport features. Figure 4a shows the conductivity as a function of T at different magnetic fields of $(Bi_2Se_3)_6/(In_2Se_3)_6$ SLs. At zero field, the conductivity shows a logarithmic T−dependence decrease at low T, which is similar to 2D TI thin films.[26,28,38] The MC behavior of $(Bi_2Se_3)_6/(In_2Se_3)_6$ SLs measured in perpendicular field is shown in Figure 4b. The nonsaturating, linear MC behavior treated as a signature for the surface transport[38−40] is observed in high field, whereas the crossover feature of 3D transport is absent. Furthermore, the MC measurements performed under parallel field configuration shown in Figure

dx.doi.org/10.1021/nl502220p | Nano Lett. 2014, 14, 5244−5249

4c display monotonic decrease instead of the crossover behavior, also in accord with MC features in 2D TI thin films.

Therefore, we suppose the $(Bi_2Se_3)_6/(In_2Se_3)_6$ SLs are more like a stack of N independent 2D layers, and simulate the conductivity as well as the MC data in the paradigm of 2D quantum transport theory. To account for the negative conductivity correction at low temperature, the 2D theory containing both WAL and EEI corrections is given by[34]

$$\Delta\sigma(T) = N\frac{e^2}{4\pi^2\hbar}\left(2\alpha p + 2 - \frac{3}{2}\tilde{F}_\sigma\right)\ln\left(\frac{T}{T_0}\right) \quad (3)$$

where the integer number N stands for the number of independent channels in the SLs system. The coefficient α is fixed to $-1/2$ for a single conducting channel in the SLs of TI layer.[5,26] T_0 is a reference temperature where conductivity starts to decline. Considering EEI is the dominant mechanism for dephasing at low T, we take $p = 1$.[34] Here, the integer number N and the screening factor $\tilde{F}_\sigma$ are the fitting parameters. The fitting results are shown by the pink dashed line in Figure 4a, and yields $N = 8$ and $\tilde{F}_\sigma = 0.5$. (See Supporting Information for details)

Moreover, the 2D paradigm is applied to interpret the MC data under both perpendicular and parallel field. The conductivity correction reads: $\Delta\sigma(H,T) = \Delta\sigma_{WAL}(H,T) + \Delta\sigma_{EEI}(H,T)$. To be specific, for the perpendicular field case, the MC corrections are given by[34,41]

$$\Delta\sigma_\perp(H,T) = \alpha N\frac{e^2}{2\pi^2\hbar}\left[\Psi\left(\frac{1}{2} + \frac{\hbar}{4eBL_\varphi}\right) - \ln\left(\frac{\hbar}{4eBL_\varphi}\right)\right] - N\frac{e^2}{4\pi^2\hbar}\tilde{F}_\sigma g_2(h) \quad (4)$$

where the first term is Hikami–Larkin–Nagaoka (HLN) formula describing the WAL correction and the second term is the 2D EEI correction with

$$g_2(h) = \int_0^\infty d\varepsilon \ln\left|1 - h^2/\varepsilon^2\right|\frac{d^2}{d\varepsilon^2}(\varepsilon/[\exp(\varepsilon/k_BT) - 1])$$

And the quantum corrections in parallel field read[34,42]

$$\Delta\sigma_\parallel(H,T) = -\frac{Ne^2}{4\pi^2\hbar}\ln\left(1 + \frac{L_\varphi^2}{L_\parallel^2}\right) - N\frac{e^2}{4\pi^2\hbar}\tilde{F}_\sigma g_2(h) \quad (5)$$

The first and second term express the 2D WAL and EEI corrections to the conductivity, respectively. $L_\parallel = 4L_B^2(l/d)^{1/2}/d$ with L_B being the magnetic length (See Supporting Information for details.)

In our analysis, given the best fitting condition, the fitting range is fixed from −0.4 to 0.4 T. The fittings to the MC data measured in the perpendicular field yields $L_\varphi = 278$ nm and $\alpha N = -4$ (shown in Figure 4b). In the TI system with a single conduction channel, α is universal and equals $-1/2$.[5,26] The WAL contributions for incoherent 2D TI channels add up to give the final MC corrections,[43] consequently, $\alpha N = -4$ means we have $N = 8$ independent parallel conducting channels in the SLs system, corresponding to approximately 80% of total Bi_2Se_3 thin-film layers. Furthermore, the best fitting for the parallel data in Figure 4c also shows the same results with $L_\varphi = 263$ nm and $N = 8$, within range of −1 to 1 T. Although the In_2Se_3 may have poor conductivity due to the intrinsic defects doping effect, the bulk states of In_2Se_3 hardly contribute to the MC correction due to its small conductivity compared with Bi_2Se_3 surface states. The consistent fitting data in $(Bi_2Se_3)_6/(In_2Se_3)_6$ SLs display a good agreement with 2D WAL and EEI theory. Thus, the thickness reduction of TI layers indeed causes significantly different interlayer coherence properties in Bi_2Se_3/In_2Se_3 SLs systems.

One unaddressed question remains: why are the transport characteristics for $(Bi_2Se_3)_{12}/(In_2Se_3)_6$ SLs and $(Bi_2Se_3)_6/(In_2Se_3)_6$ SLs considerably different? Previous experimental findings have revealed surface states hybridized in ultrathin Bi_2Se_3 films (thickness ≤ 6 QLs).[7] Moreover, first principle calculations for Bi_2Se_3/In_2Se_3 heterostructure have found that the surface states in Bi_2Se_3 penetrate slightly into the In_2Se_3 interface.[44] Thus, the surfaces states of aforementioned two TI/NI SLs samples are almost the same, indicating the discordance of transport features in these two TI/NI SLs cannot be simply attributed to surface conducting channels. In fact, a recent in-depth theoretical study, based on 2D WL theory, reveals that both bulk states and surface states jointly contribute to MC corrections in TI thin films.[43] Considering the transport results in $(Bi_2Se_3)_{12}/(In_2Se_3)_6$ SLs and $(Bi_2Se_3)_6/(In_2Se_3)_6$ SLs, we speculate that the surface states can more easily penetrate through the In_2Se_3 layers and finally form 3D energy bands for SLs with thick Bi_2Se_3 layers. This result is closely related to the properties of quantum well (QW) states in thick Bi_2Se_3 layers, and the chemical potential doping effect in the interface of In_2Se_3 and thick Bi_2Se_3 layers. In contrast, for the $(Bi_2Se_3)_6/(In_2Se_3)_6$ SLs with thinner Bi_2Se_3 layers, the scarcity of QW states, and different chemical potential doping in the interfaces hinder the coherently tunneling to other layers, and give rise to the transport features in 2D WL paradigm. Further, the first principle studies on the band structures of TI/NI SLs are needed to understand the microscopic origin of these exotic transport features. Our results reveal both TI surface states and bulk QW states, even the chemical potential doping in the interfaces influence the electronic properties of TI/NI SLs, and shed new lights on the comprehensive understanding of the Weyl semimetal phase in TI/NI SLs. In addition, the multiplied surface state channels in our artificially designed TI/NI SLs open a new way for applications such as thermoelectric and spintronics devices.[23,45]

In summary, we performed a systematic study on the transport properties of Bi_2Se_3/In_2Se_3 SLs with different thickness of TI layers. The study demonstrates that in Bi_2Se_3/In_2Se_3 SLs, the transport dimensionality—2D or 3D—is influenced by the thickness of TI layer. For $(Bi_2Se_3)_{12}/(In_2Se_3)_6$ SLs with thicker TI layers, the quantum correction to the conductivity and MC can be explained by 3D WAL theory combined with EEI, resulting from coherent 3D transport channels. For $(Bi_2Se_3)_6/(In_2Se_3)_6$ SLs with thinner TI layers, due to the less bulk bands, the layered system displays features of incoherent 2D transport channels. As the first systematic transport study on the artificial TI/NI SL systems, our work may stimulate the research on exploring exotic quantum phenomena and potential applications in TI/NI SLs.

■ ASSOCIATED CONTENT

Supporting Information

Methods, theoretical background, and fitting details. This material is available free of charge via the Internet at http://pubs.acs.org.

dx.doi.org/10.1021/nl502220p | Nano Lett. 2014, 14, 5244−5249

AUTHOR INFORMATION

Corresponding Authors

*E-mail: mhxie@hku.hk.
*E-mail: xcxie@pku.edu.cn.
*E-mail: jianwangphysics@pku.edu.cn.

Author Contributions

¶These authors contributed equally to this work.

Notes

The authors declare no competing financial interest.

ACKNOWLEDGMENTS

We acknowledge Moses H. W. Chan and Hua Jiang for fruitful discussions and Bin Li for the help in sample growth. This work was financially supported by National Basic Research Program of China (grant nos. 2013CB934600 and 2012CB921300), the National Natural Science Foundation of China (nos. 11222434, 11174007, and 11174244), and the Research Fund for the Doctoral Program of Higher Education (RFDP) of China. M.H.X. acknowledge support of the HKRGC General Research Fund (No. HKU7061/11P).

REFERENCES

(1) Qi, X. L.; Zhang, S. C. *Phys. Today* **2010**, *63*, 33−38.
(2) Hasan, M. Z.; Kane, C. L. *Rev. Mod. Phys.* **2010**, *82*, 3045−3067.
(3) Qi, X. L.; Zhang, S. C. *Rev. Mod. Phys.* **2011**, *83*, 1057−1110.
(4) Checkelsky, J.; Hor, Y.; Liu, M. H.; Qu, D. X.; Cava, R.; Ong, N. *Phys. Rev. Lett.* **2009**, *103*, 246601.
(5) Chen, J.; Qin, H. J.; Yang, F.; Liu, J.; Guan, T.; Qu, F. M.; Zhang, G. H.; Shi, J. R.; Xie, X. C.; Yang, C. L.; Wu, K. H.; Li, Y. Q.; Lu, L. *Phys. Rev. Lett.* **2010**, *105*, 176602.
(6) Analytis, J. G.; McDonald, R. D.; Riggs, S. C.; Chu, J.-H.; Boebinger, G. S.; Fisher, I. R. *Nat. Phys.* **2010**, *6*, 960−964.
(7) Zhang, Y.; He, K.; Chang, C. Z.; Song, C. L.; Wang, L. L.; Chen, X.; Jia, J. F.; Fang, Z.; Dai, X.; Shan, W. Y.; Shen, S. Q.; Niu, Q.; Qi, X. L.; Zhang, S. C.; Ma, X. C.; Xue, Q. K. *Nat. Phys.* **2010**, *6*, 584−588.
(8) Peng, H. L.; Kong, D. S.; Meister, S.; Chen, Y. L.; Qi, X. L.; Zhang, S. C.; Shen, Z. X.; Cui, Y. *Nat. Mater.* **2010**, *9*, 225−229.
(9) Hong, S. S.; Cha, J. J.; Kong, D.; Cui, Y. *Nat. Commun.* **2012**, *3*, 757.
(10) Kim, D.; Cho, S.; Butch, N. P.; Syers, P.; Kirshenbaum, K.; Adam, S.; Paglione, J.; Fuhrer, M. S. *Nat. Phys.* **2012**, *8*, 459−463.
(11) Taskin, A. A.; Sasaki, S.; Segawa, K.; Ando, Y. *Phys. Rev. Lett.* **2012**, *109*, 066803.
(12) Fang, L.; Jia, Y.; Miller, D. J.; Latimer, M. L.; Xiao, Z. L.; Welp, U.; Crabtree, G. W.; Kwok, W. K. *Nano Lett.* **2012**, *12*, 6164−6169.
(13) Wang, Z.; Qiu, R. L. J.; Lee, C. H.; Zhang, Z.; Gao, X. P. A. *ACS Nano* **2013**, *7*, 2126−2131.
(14) Tian, M.; Ning, W.; Qu, Z.; Du, H.; Wang, J.; Zhang, Y. *Sci. Rep.* **2013**, *3*, 1212.
(15) Burkov, A.; Balents, L. *Phys. Rev. Lett.* **2011**, *107*, 127205.
(16) Zyuzin, A. A.; Wu, S.; Burkov, A. A. *Phys. Rev. B* **2012**, *85*, 165110.
(17) Halász, G. B.; Balents, L. *Phys. Rev. B* **2012**, *85*, 035103.
(18) Esaki, L.; Chang, L. L. *Phys. Rev. Lett.* **1974**, *33*, 495−498.
(19) Szott, W.; Jedrzejek, C.; Kirk, W. P. *Phys. Rev. B* **1989**, *40*, 1790−1794.
(20) Nakayama, K.; Eto, K.; Tanaka, Y.; Sato, T.; Souma, S.; Takahashi, T.; Segawa, K.; Ando, Y. *Phys. Rev. Lett.* **2012**, *109*, 236804.
(21) Valla, T.; Ji, H. W.; Schoop, L. M.; Weber, A. P.; Pan, Z.-H.; Sadowski, J. T.; Vescovo, E.; Fedorov, A. V.; Caruso, A. N.; Gibson, Q. D.; Müchler, L.; Felser, C.; Cava, R. J. *Phys. Rev. B* **2012**, *86*, 241101.
(22) Gibson, Q. D.; Schoop, L. M.; Weber, A. P.; Ji, H. W.; Nadj-Perge, S.; Drozdov, I. K.; Beidenkopf, H.; Sadowski, J. T.; Fedorov, A.; Yazdani, A.; Valla, T.; Cava, R. J. *Phys. Rev. B* **2013**, *88*, 081108(R).
(23) Song, J.-H.; Jin, H.; Freeman, A. J. *Phys. Rev. Lett.* **2010**, *105*, 096403.
(24) Wang, Z. Y.; Guo, X.; Li, H. D.; Wong, T. L.; Wang, N.; Xie, M. H. *Appl. Phys. Lett.* **2011**, *99*, 023112.
(25) Jiang, Y.; Wang, Y.; Sagendorf, J.; West, D.; Kou, X.; Wei, X.; He, L.; Wang, K. L.; Zhang, S.; Zhang, Z. *Nano Lett.* **2013**, *12*, 28516.
(26) Wang, J.; DaSilva, A.; Chang, C.-Z.; He, K.; Jain, J.; Samarth, N.; Ma, X.-C.; Xue, Q.-K.; Chan, M. *Phys. Rev. B* **2011**, *83*, 245438.
(27) Liu, M.; Chang, C.-Z.; Zhang, Z. C.; Zhang, Y.; Ruan, W.; He, K.; Wang, L.-L.; Chen, X.; Jia, J.-F.; Zhang, S.-C.; Xue, Q.-K.; Ma, X. C.; Wang, Y. Y. *Phys. Rev. B* **2011**, *83*, 165440.
(28) Chen, J.; He, X. Y.; Wu, K. H.; Ji, Z. Q.; Lu, L.; Shi, J. R.; Smet, J. H.; Li, Y. Q. *Phys. Rev. B* **2011**, *83*, 241304(R).
(29) Liu, M.; Zhang, J. S.; Chang, C.-Z.; Zhang, Z. C.; Feng, X.; Li, K.; He, K.; Wang, L.-L.; Chen, X.; Dai, X.; Fang, Z.; Xue, Q.-K.; Ma, X. C.; Wang, Y. Y. *Phys. Rev. Lett.* **2012**, *108*, 036805.
(30) Cha, J. J.; Claassen, M.; Kong, D.; Hong, S. S.; Koski, K. J.; Qi, X.-L.; Cui, Y. *Nano Lett.* **2012**, *12*, 4355−4359.
(31) Zhang, D.; Richardella, A.; Rench, D. W.; Xu, S.-Y.; Kandala, A.; Flanagan, T. C.; Beidenkopf, H.; Yeats, A. L.; Buckley, B. B.; Klimov, P. V.; Awschalom, D. D.; Yazdani, A.; Schiffer, P.; Hasan, M. Z.; Samarth, N. *Phys. Rev. B* **2012**, *86*, 205127.
(32) Lang, M.; He, L.; Kou, X. F.; Upadhyaya, P.; Fan, Y. B.; Chu, H.; Jiang, Y.; Bardarson, J. H.; Jiang, W. J.; Choi, E. S.; Wang, Y.; Yeh, N.-C.; Moore, J.; Wang, K. L. *Nano Lett.* **2012**, *13*, 48−53.
(33) Zhang, L.; Dolev, M.; Yang, Q. I.; Hammond, R. H.; Zhou, B.; Palevski, A.; Chen, Y.; Kapitulnik, A. *Phys. Rev. B* **2013**, *88*, 121103.
(34) Lee, P. A.; Ramakrishnan, T. V. *Rev. Mod. Phys.* **1985**, *57*, 287−337.
(35) Kawabata, A. *J. Phys. Soc. Jpn.* **1980**, *49*, 628−637.
(36) Baxter, D. V.; Richter, R.; Trudeau, M. L.; Cochrane, R. W.; Strom-Olsen, J. O. *J. Phys. (Paris)* **1989**, *50*, 1673−1688.
(37) Bergmann, Gerd *Phys. Rep.* **1984**, *107*, 1−58.
(38) Zhao, Y.; Chang, C. Z.; Jiang, Y.; DaSilva, A.; Sun, Y.; Wang, H.; Xing, Y.; Wang, Y.; He, K.; Ma, X. C.; Xue, Q.-K.; Wang, J. *Sci. Rep.* **2013**, *3*, 3060.
(39) Tang, H.; Liang, D.; Qiu, R. L. J.; Gao, X. P. A. *ACS Nano* **2011**, *5*, 7510−7516.
(40) Wang, C. M.; Lei, X. L. *Phys. Rev. B* **2012**, *86*, 035442.
(41) Hikami, S.; Larkin, A. I.; Nagaoka, Y. *Prog. Theor. Phys.* **1980**, *63*, 707−710.
(42) Dugaev, V. K.; Khmelnitskii, D. E. *Sov. Phys. JETP* **1984**, *50*, 1038−1041.
(43) Garate, I.; Glazman, L. *Phys. Rev. B* **2012**, *86*, 035422.
(44) Zhang, Q.; Zhang, Z.; Zhu, Z.; Schwingenschlögl, U.; Cui, Y. *ACS Nano* **2012**, *6*, 2345−2352.
(45) Müchler, L.; Casper, F.; Yan, B. H.; Chadov, S.; Felser, C. *Phys. Status Solidi RRL* **2013**, *7*, 91−100.